Heterogeneity in warm-season land-atmosphere coupling over the U.S. Southern Great Plains

Qi Tang[1], Shaocheng Xie[1], Yunyan Zhang[1], Thomas J. Phillips[1], Joseph A. Santanello[2], David R. Cook[3], Laura D. Riihimaki[4], and Krista L. Gaustad[4]

[1]Lawrence Livermore National Laboratory, Livermore, California, USA

[2]NASA Goddard Space Flight Center, Greenbelt, Maryland, USA

[3]Argonne National Laboratory, Lemont, Illinois, USA

[4]Pacific Northwest National Laboratory, Richland, Washington, USA

Abstract

Heterogeneity in warm-season (May-August) land-atmosphere (LA) coupling is quantified with the long-time, multiple-station measurements from the U.S. Department of Energy Atmospheric Radiation Measurement (ARM) program and the moderate-resolution imaging spectroradiometer (MODIS) satellite remote sensing at the Southern Great Plains (SGP). We examine the coupling strength at 7 additional locations with the same surface type (i.e., pasture/grassland) as the ARM SGP central facility (CF). To simultaneously consider multiple factors and consistently quantify their relative contributions, we apply a multiple linear regression method to correlate the surface evaporative fraction (EF) with near-surface soil moisture (SM) and leaf area index (LAI). The observations show moderate to weak terrestrial segment LA coupling with large heterogeneity across the ARM SGP domain in warm-season. Large spatial variabilities in the contributions from SM and LAI to the EF changes are also found. The coupling heterogeneities appear to be associated with differences in land use, anthropogenic activities, rooting depth, and soil type at different stations. Therefore, the complex LA interactions at the SGP cannot be well represented by those at the CF/E13 based on the metrics applied here. Overall, the LAI exerts more influence on the EF than does the SM due to its overwhelming impacts on the latent heat flux. This study complements previous studies based on measurements only from the CF and has

important implications for modeling LA coupling in weather and climate models. The multiple linear regression provides a more comprehensive measure of the integrated impacts on LA coupling from several different factors.

1. Introduction

Land-atmosphere (LA) coupling has been identified to play an important role in both current (Betts, 2004, 2009; Ferguson et al., 2012; Koster et al., 2004; Taylor, de Jeu, et al., 2012) and future climate (Dirmeyer et al., 2012, 2013; Seneviratne et al., 2006) through its impacts on the energy and water cycles (Seneviratne et al., 2010 and references therein) in the Earth climate system. Numerous studies aim to evaluate and quantify the overall strength or the degree of LA coupling (e.g., Koster et al., 2002, 2006) as well as its individual interactions and feedback components (e.g., Dirmeyer, 2011; Wei & Dirmeyer, 2010) using numerical models (e.g., general circulation models, land surface models, and single column models) and observations (in situ, ground and satellite remote sensing). However, the driving mechanisms of how the land states (e.g., soil wetness and vegetation) impact the surface turbulent fluxes (i.e., latent and sensible heat fluxes) to the atmosphere are not well understood. Classical hydrology (Budyko, 1974) provides conceptual first-order definitions of evapotranspiration (ET) regimes and predicts strong coupling at dry-wet transitional zones due to soil moisture-limited conditions. These coupling “hot spots” are confirmed by multiple-model experiments in an ensemble-mean sense (Koster et al., 2004; Seneviratne et al., 2006). The United States (US) Southern Great Plains (SGP) is identified as one of these coupling hot spots in terms of the relationship between soil moisture (SM) and precipitation. Note that large inter-model differences exist for individual model results (e.g., Fig. 1 in Koster et al., 2004) and suggest large uncertainties in the simulated SM-precipitation interactions.

Observational constraints are required to evaluate how well these SM-precipitation coupling hot spots are represented in the model and to provide insights to reduce modeling uncertainties in the coupling. Land-atmosphere coupling is recognized as a two-segment process: land states link to surface fluxes (the terrestrial leg); and surface fluxes connect to atmosphere states (the atmospheric leg) (Guo et al., 2006; Santanello et al., 2011). The terrestrial leg is a critically important part of the larger SM-precipitation loop. Several recent studies focus on establishing observational evidence of the terrestrial coupling strength at the SGP with daily average data collected by the US Department of Energy Atmospheric Radiation Measurement (ARM) program. This observational evidence of the terrestrial component of LA coupling, especially the relative contributions from different factors, is largely confined to the SGP central facility (CF) due to the paucity of coincident land/soil and atmosphere observations. Based on long-term (1997-2008) ARM program observations at the SGP CF site near Lamont, Oklahoma, Phillips & Klein (2014) found that during the May-August warm season, the coupling between the top-layer (10 cm) SM and the surface evaporative fraction (EF, the ratio of latent heat (LH) flux to the sum of latent and sensible heat (SH) fluxes) is modest, as measured by the contemporary covariance ($r = 0.48$). Using observations at two adjacent sites (near the CF), however, Williams & Torn (2015) estimated much stronger ($r = 0.81$) LA coupling at the SGP by replacing SM with the leaf area index (LAI) in the conventional r(SM, EF) metric, thus highlighting the significant impact of vegetation. More recently Bagley et al. (2017) demonstrated with the ARM data that the surface energy partitioning was greatly influenced by the green leaf area on the two major SGP land covers (grassland and winter wheat). Their statistical analysis at the CF identified the LAI as the most important driver of the EF among various factors, including the near-surface SM. Phillips et al. (2017) reported substantial variabilities in the LA coupling with the r(SM, EF) metric when extending their analysis from the SGP CF site to multiple nearby (up to 150 km) ARM extended sites.

All the above observational studies emphasize the daily mean EF, which has great implications for different SGP cloud regimes (Zhang & Klein, 2013). The long-standing SGP summertime warm and dry biases in climate models are related to the surface energy biases and the LA coupling (Klein et al., 2006). Recent research (Ma et al., 2018) separated the land (EF) vs. atmosphere (radiation) contributions to the surface temperature biases, and found larger land contributions in most of the Coupled Model Intercomparison Project Phase 5 (CMIP5) (Taylor, Stouffer, et al., 2012) Atmospheric Model Intercomparison Project (AMIP) simulations. The studies by Ma et al. (2018) and Van Weverberg et al. (2018) highlight the critical role that the terrestrial coupling segment plays in this climate modeling puzzle.

In the present work, we extend the CF-centric observational studies in literature to multiple ARM SGP sites. The goal is to provide more robust and comprehensive, observationally based warm-season estimates of the terrestrial segment LA coupling strength at the SGP, and to determine how well the ARM SGP-CF measurements represent the coupling over the SGP domain. This study is motivated by the need to improve current knowledge of the driving mechanisms of daily mean EF variations, and to provide novel observational constraints on modeling physical processes of the terrestrial coupling segment at the SGP. In Section 2, we describe the sites, data, as well as the methods used in this study. In Section 3, we first show the spatial variations in the analyzed coupling variables, then quantify the strength of coupling with the EF and the turbulent fluxes at different locations, as well as the relative contributions of the SM and the LAI. Section 4 provides further discussions on the enhanced LA coupling metric, followed by sensitivity analysis of LA coupling to flux fetch, temporal averaging scale, and dry vs. wet years in Section 5. The discussions and conclusions are summarized in Section 6.

2. Sites, data, and methods

2.1 Sites

The ARM Climate Research Facility provides comprehensive observations of important atmosphere, surface, and land/soil variables to the climate research community. At the SGP, ARM deploys a dense surface network with multiple observational stations within a 3.5°x3.5° domain centered at the central facility (CF). The site locations reflect heterogeneity in land cover, vegetation types, soil types etc. More importantly, many of these ARM sites provide coincident measurements of soil moisture, LH and SH fluxes, which offer a unique opportunity to study the terrestrial component of LA coupling. To minimize the number of impacting factors and enhance the robustness of analyses, we opted to use 8 sites (see Fig. 1 and Table 1), including the CF (i.e., E13), located on the same land cover (pasture/grassland) with relatively complete long-time, coincident measurements from the same instruments (i.e., Energy Balance Bowen Ratio (EBBR) systems). Differences among the 8 sites (see Table 1) include grass species, human activities (e.g., grazed vs ungrazed), and soil types.

2.2 Data

In this study, we use the hourly averaged SM (at 2.5-cm depth), surface LH and SH fluxes in the warm season (May—August) of years 2004-2011 from the ARM Best Estimate (ARMBE) (Xie et al., 2010) station-based surface data (ARMBESTNS) (Tang & Xie, 2015b) (https://www.arm.gov/capabilities/vaps/armbestns, doi: 10.5439/1178332). Soil moisture, LH and SH fluxes are measured by EBBR systems (Cook, 2018). Following Betts (2009) and Phillips & Klein (2014), our analyses emphasize daily averages, but also include the sensitivity to different temporal averaging intervals. The daily mean SM is calculated from 00:00 to 23:00 UTC, and the daily daytime mean of the EF from 12:00 to 23:00 UTC (6:00 to 17:00 LST). Leaf area index (LAI) is from the MCD15A3H (version 6) data product (Myneni, 2015) (https://lpdaac.usgs.gov/dataset_discovery/modis/modis_products_table/mcd15a3h_v006, doi: 10.5067/MODIS/MCD15A3H.006), which combines the measurements from the two moderate-resolution imaging spectroradiometer (MODIS) instruments on NASA satellites Terra and Aqua to create a 4-day composite data set at a 500 m horizontal resolution. The LAI of the pixels closest to the ARM stations (see Fig. 1) are used in our site-specific analyses. Ideally, we need the LAI that matches the footprint (about 100 m x 100 m) of EBBR flux measurements. Such high-resolution LAI data require ground-based measurements, which are not available. Figure 1 also shows the mean warm-season geographic patterns of EBBR SM and MODIS LAI for the years 2004—2011. The latitude-longitude SM data are taken from the ARMBE 2-dimensional Gridded Surface data (ARMBE2DGRID) (Tang & Xie, 2015a) (https://www.arm.gov/capabilities/vaps/armbe2dgrid, doi: 10.5439/1178331), which interpolates the station-based ARMBESTNS data to a 0.25° x 0.25° grid over the SGP domain (35°N—38.5°N and 95.5°W—99.5°W) with the Barnes scheme (Barnes, 1964). Both patterns in Fig. 1 display a general increasing gradient from northwest to southeast.

2.3 An enhanced land-atmosphere coupling metric

For the terrestrial segment, the correlation between top-layer soil water content and the EF focuses on the influence of bare soil evaporation, whereas the correlation between the LAI and the EF emphasizes the impact of evapotranspiration (ET) from vegetation, which is largely controlled by the soil moisture in the root zone rather than near the surface. Since on a daily or longer scale surface net radiation is roughly balanced by the sum of LH and SH fluxes (neglecting ground heat storage), we can focus on the LH flux and infer the SH flux from the surface energy balance. The surface LH flux consists of two major components: evaporation from bare soil, and ET by plants (Seneviratne et al., 2010). A robust coupling metric is expected to simultaneously capture the contributions from multiple factors, as the coupling processes occur at the same time in reality. However, the traditional simple correlation metrics examine interactions between pairs of variables, such as SM-EF, SM-SH flux, SM-lifting condensation level, SM-planetary boundary layer height, LAI-EF, etc. (Betts, 2009; Ford et al., 2014; Phillips & Klein, 2014; Santanello et al., 2007; Williams & Torn, 2015), and hence are only able to quantify the influence from one factor at a time, in a partial derivative sense. In this study, we instead employ a multiple linear regression method to study the integrated impact of top-layer SM and vegetation to the surface energy partitioning. Although it would be desirable to incorporate in root-zone SM due to its obvious connection to the transpiration, root-zone SM measurements are not available at the selected 8 sites. Williams & Torn (2015) examined the soil-depth dependency of the SM coupling with EF at an SGP grass site, and only found a slight increase in the SM-EF correlation with increasing depth. It is reasonable to assume that similar soil-depth dependency in r(SM, EF) applies to the 8 SGP grassland sites analyzed here, and that the SM dependency is largely captured by our multiple linear regression model.

Multiple linear regression reveals the relationship between two or more explanatory or predictor variables and a response variable by fitting a line through data points in a least squares sense. Previous studies (e.g., Betts et al., 2015) applied multiple linear regression to study the coupled LA system on daily timescales. The novelties of the present work are the application to the relationships between EF or the turbulent fluxes and SM and LAI, and to quantify the relative importance of SM versus LAI coupling (see details below). To account for the impacts of soil moisture and vegetation on the partition of surface turbulent fluxes simultaneously, we construct the following multiple linear regression:

$$EF = b(0) + b(1) * SM + b(2) * LAI \quad (1)$$

where b is the partial regression coefficient. It should be noted that while not a mathematical pre-condition, it is important to use independent or weakly correlated predictor variables in the regression model to ensure that the multiple linear regression is applied in a physically meaningful way. To this end, it is necessary to examine the dependencies between predictor variables before applying the multiple linear regression metric. The LA coupling strength is defined as the multiple correlation coefficient (Kutner et al., 2004)

$$R = \frac{\sqrt{r^2(EF,SM)+r^2(EF,LAI)-2*r(EF,SM)*r(EF,LAI)*r(SM,LAI)}}{\sqrt{1-r^2(SM,LAI)}} \quad (2)$$

in which r denotes the Pearson's correlation coefficient between two variables. The multiple regression Eq. 1 can be extended to more than two predictor variables (see Supporting Information), and hence can include other potentially important variables. By adding more variables to the regression, no matter whether significantly correlated with the EF or not, R will always increase by definition. Therefore, one cannot determine the importance of a newly added variable, based merely on an enhanced R value. This limitation is addressed by examining the standardized regression coefficient and its significance test, as follows.

The multiple regression and correlation quantify the combined effects of the SM and LAI to the EF. Moreover, these tools allow us to disentangle and examine their separate influence on the EF (see Section 3.2.2 for more details). The standardized regression coefficients

$$B_i = b_i * \sigma_{x_i}/\sigma_y \quad (3)$$

can be used to evaluate the sensitivity of the variability in the EF (i.e., σ_y in Eq. 3) to the variation in the SM or the LAI (i.e., σ_{xi} in Eq. 3), respectively, where σ denotes the standard deviation. For simple regression (i.e., only one predictor variable), the standardized regression coefficient is identical to the correlation coefficient r. It is also helpful to define the sensitivity index ($I = b*\sigma_x$) to quantify the potential of soil moisture oscillations to cause variations in surface fluxes (Dirmeyer, 2011). For multiple regression, the sensitivity index (I) can still be used to assess the relative influence from different predictors at the same location, but it cannot be applied across different locations because the least squares fitting depends on the EF observations, which change with location. The standardized regression coefficient (B) breaks this limitation of I by considering the standard deviations in both the predictor and response variables, and thus it can be directly compared among different variables at different locations to quantify the spatial variability of their relative importance to the EF fluctuation.

The soil moisture index (SMI) [$SMI = (SM - SM_{min})/(SM_{max} - SM_{min})$] is useful to study the correlation with the EF (Betts, 2009; Phillips & Klein, 2014), facilitating comparisons between sites with different soil and vegetation types, and hence different field wetness capacity and wilting point. In this study, because years 2004—2011 cover a wide range of wet and dry conditions, we approximate the SMI at each station using the multiyear local maximum (SM_{max}) and minimum (SM_{min}) for field capacity and wilting point, respectively. Note that the correlation coefficients remain the same no matter whether SM or SMI is used.

The statistical significance of the multiple regression is assessed using the variance analysis together with the two-tailed F-test. The significance of partial regression coefficients is examined by the two-tailed t-test. The significance of the difference between two correlation coefficients is tested with the Fisher's r to z transformation (Fisher, 1921) and the null hypothesis of $p1 – p2 = 0$. In all cases, a significance level of $p = 0.05$ (95% confidence level) is used. The degrees of freedom are assumed as (N-2) in the t-test and as (N-3) in the F-test and the Z-test. These degrees of freedom take into account the possible serial correlation in the time series of observations in a similar way as in previous studies (Dirmeyer et al., 2012; Phillips & Klein, 2014), for example the N numbers in Table 1 pertain to sampling once every four days. (Missing values in coincident measurements of SM or turbulent fluxes will lower the sampling frequency.)

3. Results

3.1 Spatial variabilities in LA coupling related variables

Figure 2 shows the Taylor diagrams (Taylor, 2001), a concise summary of how closely one dataset matches the other, for observations of important LA coupling variables (i.e., LH, SH, EF, SM, and LAI) at the extended SGP sites relative to the CF. The mean biases in the Taylor diagrams are denoted by the size and shape of the symbols in addition to the three statistics – the temporal correlation (angle), the normalized standard deviation (radius, normalized by that of the CF), and the normalized centered root-mean-square (RMS) difference (distance to the (1, 0) reference point, also normalized by the corresponding CF value). The more similar the extended observations are to those at the CF, the closer their symbols are to the (1, 0) point. The spread of SGP sites on the same Taylor diagram reveals the spatial heterogeneity at those locations.

In general, these important LA coupling variables at most of the ARM extended sites have a rather weak correlation (< 0.6) and large RMS differences from those measured at the CF. Large RMS differences are indicated by the large distances between the data points and the reference point in Fig. 2. The variance of these variables also shows large differences from that measured at the CF. All the sites show a smaller standard deviation in SH and EF than at CF. Among these variables, the LAI (Fig. 2e) shows the least similarities to that at the CF: weak correlations (statistically insignificant at E4 and E7) and large variances (off the chart at E7 and E12), suggest that the LAI is the most localized property. There also are quite large differences in these statistics across different sites.

3.2 Heterogeneity in LA coupling strength

Large spatial heterogeneities in the individual measurement of the coupling variables do not automatically translate to great spatial variations in the coupling strength among these variables. In this section, we examine the terrestrial segment of the LA coupling strength at the 8 SGP stations, as estimated by the traditional simple regression metrics and by the multiple regression metric. The results of simple regression methods facilitate comparisons with previous studies, whereas the multiple regression metric provides new insights by overcoming some limitations of the conventional metrics (see Section 2.3 for details).

3.2.1 Strength of coupling with the evaporative fraction at different SGP sites

The evaporative fraction (EF) plays a crucially important connection role between the land surface properties and the atmospheric states. It has great impacts on the atmospheric boundary layer conditions (Findell et al., 2011; Williams & Torn, 2015), and hence processes (e.g., convection, clouds, and precipitation) in the free atmosphere (Findell & Eltahir, 2003; Gentine et al., 2013). We first compare the summertime coupling strength with the EF at 8 ARM SGP stations assessed with 3 different metrics (see Fig. 3). To make consistent comparisons, we use only the data when measurements of all 3 variables (i.e., EF, SMI, and LAI) are available. The surface and soil types of these 8 stations are summarized in Table 1. The LA coupling strength is examined by using the daily anomalies of EF, SMI, and LAI relative to the climatological monthly means of years 2004--2011. We, therefore, minimize the impact of seasonal covariations, such as that between the EF and the LAI, on these temporal correlation-based coupling estimations. The daily to sub-monthly and inter-annual variabilities are retained by this process. As a result, variables in Fig. 3 have both positive and negative values. Note that from a physical point of view, it is important to use independent or weakly correlated predictor variables (i.e., right side variables of Eq. 1 and S1) in the multiple linear regression method. The fourth column of Table 1 verifies that the correlations between the top-layer SM and the LAI at 8 SGP stations are generally very weak (mostly below $r = 0.20$, three of which are not statistically significant). This suggests that the application of the multiple linear regression method is justified.

First, focusing on the CF site, our result confirms that there is only a moderate correlation between the EF and the SMI plotted as a scatter diagram in Fig. 3a. A positive correlation indicates an SM-limited regime. However, our correlation coefficient ($r = 0.41$) is smaller than those estimated in previous studies, such as 0.48 in Fig. 5a of Phillips & Klein (2014) and 0.46 in Fig. 1a of Williams & Torn (2015). Such small differences in the correlation coefficients are not statistically significant. There are three major reasons for these differences: 1) Whether or not the climatological monthly means are removed; 2) Data measured by different instruments at different depths (e.g., 2.5-cm EBBR in the present study vs. 10-cm Soil Water And Temperature System (SWATS) SM in Phillips & Klein (2014) and Williams & Torn (2015)); and 3) Analysis of different time periods, during which large inter-annual variations exist in r(EF, SMI) (Ford et al., 2014). The moderate SM-EF correlations suggest that the top-layer (2-10 cm below the surface) SM only partly drives the changes in the EF at the CF. In addition, retaining the monthly climatological means weakens the correlation to $r = 0.37$ in our calculation. Similar slight correlation reductions (mostly statistically insignificant) are generally found at other extended sites by retaining the monthly means, implying weaker EF-SM covariations on the seasonal scale than on the daily scale.

Substituting LAI for SMI in the correlation with the EF, Fig. 3b illustrates a slightly enhanced correlation ($r = 0.42$) at the CF. This result is consistent with the conclusion of Williams & Torn (2015) that vegetation plays an important role in the LA coupling at the CF. It is worth noting that the r(EF, LAI) is much smaller with the satellite LAI in Fig. 3b than with the ground-based LAI ($r > 0.7$ found by Williams & Torn (2015) and Phillips et al. (2017). This difference suggests that the uncertainties in the coarse satellite-retrieved LAI can cause an uncertainty of ± 0.3 in r(EF, LAI). We then employ the new application of multiple linear regression (Eq. 1) to quantify the integrated influence of SM and

LAI on the EF (see Fig. 3c). The multiple correlation coefficient (R = 0.51) is larger than both simple correlations. In addition, both partial regression coefficients (b(1) and b(2) in Eq. 1) are statistically significant at the 95% level. These results suggest that both SM and vegetation are important factors in the LA coupling at the CF and their combined impact is greater than individual ones. Existing metrics, e.g., r(EF, SMI) and r(EF, LAI), only consider parts of the processes involved in the coupled system, and hence both underestimate the coupling strength. Applying the sensitivity index (I) with the partial regression coefficients of SMI and LAI, respectively, we find that vegetation plays a slightly more important role than the SM in affecting the partition of surface turbulent fluxes at the CF.

Next, we expand our analysis to the ARM extended facilities (see Fig. 3d-x) to examine the spatial variability of LA interactions across the SGP region. These extended stations are in the mesoscale vicinity (60--167 km) of the CF. Large spatial variabilities are found across the small SGP domain in all 3 metrics. The correlations range from insignificantly small (E9, Fig. 3j and E12, Fig. 3m) to 0.55 (E20, Fig. 3v) for r(EF, SMI), 0.19 (E9, Fig. 3k) to 0.51 (E20, Fig. 3w) for r(EF, LAI), and 0.23 (E9, Fig. 3l) to 0.70 (E20, Fig. 3x) for R(EF; SMI, LAI). It is noted that the coupling strength at the CF is modest among these stations by all three metrics. These results suggest that generally the coupling strengths assessed with different correlation coefficients qualitatively agree with each other. Note that the grass at the CF has been ungrazed for a long time (23 years) and has been mowed, resulting in denser and healthier vegetation than at other grassland locations, except E12. At E12, the EF-SMI coupling is insignificant, and thus the coupling at E12 is insensitive to the 2.5-cm SM. EF and LAI are marginally correlated at E12, however, because the tall grass prairie vegetation has much deeper roots than the grazed or ungrazed pasture cover that are common at other stations. Other factors, such as human activity (whether to graze or not) and soil type, may also contribute to the differences between different stations. In summary, the LA coupling across the SGP region is quite heterogeneous, with moderate coupling at the CF. These results suggest that the LA coupling at CF may not be representative of that across the SGP domain.

3.2.2 Relative contributions from SM and LAI to EF at different SGP locations

Besides the coupling strength, it is important to identify the relative contributions from various factors, such as the SM and the LAI, based on observations. Such information provides critical guidance to improve the representation of the LA coupling in weather and climate models. As described in Sect. 2.3, the multiple regression metric calculates the standardized regression coefficients (B) for the SMI and the LAI, respectively. The importance of the SMI vs. the LAI to the coupling with EF is diagnosed by the relative magnitudes of these B coefficients.

The B_{SMI} and B_{LAI} values at different stations are labeled in the third column of Fig. 3. Surprisingly different from the traditional view, but consistent with the recent studies of Williams & Torn (2015) and Bagley et al. (2017), the EF of the majority (6 out of 8) of these stations show stronger correlations with LAI than with SM. These results emphasize the importance of vegetation impacts on the EF via stomatal controls on transpiration at these grassland SGP stations. These results also suggest that bare soil evaporation (tightly correlated to the top-layer SM) contributes less to the LH flux than does ET by vegetation, which is more controlled by the root zone SM. There is apparent association between the root zone and the top-layer soil wetness, but the degree may vary depending on the soil and vegetation types. Moreover, photosynthesis is not only controlled by the root zone SM. Other factors, such as leaf temperature, solar radiation, relative humidity, and carbon dioxide concentration, also influence photosynthesis (Govindjee, 2012), and hence the ET through plants. Due to these additional factors, our results imply different degrees of decoupling between top-layer vs. root-zone SM controls on the EF at stations surrounding the CF.

The two stations (E7 and E20) where the EF is more strongly coupled to SM than LAI are located on pasture and silty loam soil. With the same soil type (silty loam), but ungrazed pasture vegetation, the LA coupling is more influenced by the LAI than by the SM at E19, or is influenced nearly the same by both factors at the CF. It is expected that bare soil evaporation becomes more important than ET by plants after grazing occurs. These results suggest that anthropogenic activities might play an important role in affecting the LA coupling. Additionally, at E7 the sensitivity of the EF to the SM (I_{SMI} = 0.04) is 2 times larger than that of the LAI (I_{LAI} = 0.02). This sensitivity difference would be underestimated as 1.3 times if simple correlations were used, because the regression slopes change with the regression model when the explanatory variables (SMI and LAI in this case) are not totally independent of each other. Therefore, the multiple regression metric shows advantages over the single-variable metric in assessing the sensitivities of EF to either SM or LAI by taking into account the weak correlations between SM and LAI.

More importantly, the standardized regression coefficient can be used to compare the sensitivities of the EF to the SM or the LAI at different places, and therefore to evaluate the spatial variability of the SM and the LAI contributions. For example, it is interesting to compare the SM sensitivities at the extended facilities to that at the CF. Both the single and multiple variable metrics (see Fig. 3, first and third columns) reveal qualitatively consistent results of modest SM sensitivity at the CF amongst the analyzed ARM stations. Overall, the third column of Fig. 3 exhibits a wide spatial range of contributions of the SM and the LAI: from statistically insignificant B_{SMI} at E9 and E12 to a maximum of B_{SMI} = 0.49 at E20. The CF numbers fall within the ranges of both B_{SMI} and B_{LAI} over the other ARM SGP stations.

3.2.3 Strength of domain-mean coupling with evaporative fraction

Given the large spatial variability in LA coupling strength across the ARM SGP domain, information from a single station may not be suitable for evaluating global climate models because model results represent means over a model grid box with a typical scale of 100 km. The single point measurement will be more useful when parameterization schemes can better represent the sub-grid variability in models in the future. To examine the coupling strength over the SGP domain, we repeat the same analysis on the domain-mean values of EF for the 8 stations (see Fig. 4). The points are less dispersed on the EF-LAI scatter plot (Fig. 4b) than on the EF-SMI plot (Fig. 4a). Consequently, the mean EF is correlated more with the mean LAI (r(EF, LAI) = 0.52) than with the mean SMI (r(EF, SMI) = 0.39). The correlation further increases to R=0.60 with the multiple variable regression. In other words, 36% (R^2) of the mean EF variance can be explained by the mean SM and LAI together. As for the sensitivities, the mean EF is more responsive to the mean changes in the LAI than in the SM, no matter which metric is used. As shown in Figs. 3 and 4, it is evident that the measurements at the CF cannot well represent the domain-mean LA coupling over the SGP region, due to the great spatial heterogeneity. Given the important role that vegetation plays in the domain-mean LA interactions, it is critical for models to better simulate the vegetation impacts on LA coupling.

3.2.4 Coupling with turbulent fluxes

Understanding which factor (LH or SH) dominates the EF variances can provide valuable information on the surface energy partitioning and some guidance for model development. Although the driving processes of LH and SH fluxes are largely connected, the physical processes are often represented by different parameters or parameterizations in the model (Moene & van Dam, 2014; Oleson et al., 2013). Observational evidence separating the impacts on these two fluxes on the LA interactions will be more likely to shed light on how to improve the LA coupling in the model. In this section, we replace EF with LH and SH in the multiple regression model (Eq. 1) to examine how the SM and the LAI interact with each of these two turbulent fluxes respectively.

The multiple regression results for the LH and the SH are shown in Figs. 5 and 6. As the SGP is a SM-limited area in summer, the slopes of the LH fitting line are positive and thus negative for the SH fitting lines. The coupling strength generally decreases when switching from the EF (see Fig. 3 third column) to turbulent fluxes, except for the E9 site. The coupling strengths with the LH and the SH both vary from statistically insignificant to R = 0.57, but the weakest and strongest interactions occur at different locations: E7 and E20 for the LH, and E9 and E19 for the SH. The minimum and maximum coupling locations are also different from those for the EF: E9 and E20, resulting from the competing relationship between the LH and the SH in determining the EF.

All the sites (except for E7 with insignificant statistics) and the domain mean (Fig. 5i) show larger contribution from the LAI than from the SM to the LH variance (see Fig. 5). Moreover, only 2 sites (E4 and E20) have statistically significant SM contributions to the LH. Over SGP grassland, it is obvious that the impact on EF by ET dominates over bare-soil evaporation. As for the SH (see Fig. 6), the SM and the LAI show comparable impacts: almost half the sites are SM-dominant and the remaining are LAI-dominant. The SM exerts stronger control on the SH domain average than does the LAI. Therefore, the overall greater control of the LAI on the EF is largely through its overwhelming influence on the LH. Regarding the spatial patterns, Figures 5 and 6 demonstrate similarly large variations in the strength of the coupling with turbulent fluxes compared to that with EF (refer to Fig. 3). The coupling strength at the CF is also moderate relative to other analyzed SGP locations.

4. Further discussion of the enhanced LA coupling metric

We have demonstrated a new application of multiple linear regression to enrich the current arsenal of land-atmosphere (LA) coupling metrics. Since the LA coupling strength reflects the integrated effect of interactions between the surface and the atmospheric boundary layer (Ek & Holtslag, 2004), compared to traditional single-variable metrics, one obvious advantage of this new application is that it provides a more comprehensive measure of the integrated impacts of multiple factors such as soil moisture or vegetation on variables such as EF or turbulent fluxes. By taking into account the standard deviations in both the predictor and response variables, the standardized regression coefficient (B) exceeds the sensitivity index (I) as a means to separate the impacts of each individual driver, and quantify the spatial patterns of their relative contributions to the overall coupling strength. We argue that the standardized regression coefficient is closer to reality since it reflects multiple impacts, and thus is a better measure than the conventional simple regression-based sensitivity. By examining the cumulative influences from all factors, we could renew or confirm our current understanding of the controlling mechanisms of the coupling for different locations and times. Since the new multiple linear regression application evaluates different mechanisms in a consistent manner, it overcomes the possible inconsistency that would otherwise arise in the application of single-variable regression, due to the dependencies among the explanatory variables. Moreover, besides near-surface SM and LAI, we can include more predictor variables (e.g., root-zone SM or other atmosphere variables) in the regression model. The left side of the regression model is also flexible. The general matrix forms of Eq. 1, the regression coefficients, and the multiple correlation coefficient are given in the Supporting Information. While here we demonstrate the application of multiple linear regression to the terrestrial segment of LA coupling, it is worth noting that this method can also be applied to the atmospheric segment, or to both the terrestrial and atmospheric segments.

5. Coupling sensitivity to flux fetch, temporal averaging scale, and dry vs. wet years

The terrestrial component of LA coupling strength assessed from observations is expected to be sensitive to a number of factors, such as the turbulent flux fetch, the temporal averaging length, and dry vs. wet years (Qian et al., 2013). It is useful to demonstrate the sensitivity of multiple linear regression metrics to these factors. More importantly, we would like to verify the robustness of large heterogeneities in LA coupling over pasture/grassland revealed in previous sections by incorporating these factors.

The accuracy of EBBR flux measurements depends on wind direction, because the fetch can be insufficient for some directions at most sites (Cook, 2018). Table 1 last column lists the wind directions for which there is sufficient grassland to ensure high quality flux measurements. The multiple linear regression coefficients R(EF; SMI, LAI) calculated without and with the wind direction filter are plotted in the first and second columns in Fig. 7a. Both columns use the daily means on the days when the data for all 3 quantities are available. It should be noted that to make consistent comparisons with other columns for longer averaging intervals, here we do not remove the climatological monthly averages as in previous sections. The impacts of applying the wind direction filter on the correlations are small at all locations with the largest change from R=0.67 to R=0.54 at E4. Although there are some subtle changes in the relative magnitude at different sites, the overall spatial variation of the LA coupling as indicated by the spread of R values remains almost the same after filtering out the degraded flux data. The corresponding standardized regression coefficients (B_{SMI} and B_{LAI}) of 1-day averaging length are shown in Fig. 7b. Color symbols represent results with the wind direction filter, while black symbols indicate those without the wind direction filter. Since the sign of B values can be arbitrary when they are statistically insignificant, we plot their absolute values in Fig. 7b. Similar to R values, the B values are not sensitive to the wind filter. The vegetation still shows stronger influence than the SM on the LA coupling strength at all sites except E7 and E20. At E20, the relative importance of the

LAI and SM to the coupling changes whether surface fluxes are filtered with wind directions (Fig. 7b) or whether the climatological monthly averages are removed (see Fig. 3x and Fig. 7b).

The terrestrial segment of LA coupling occurs at various time scales. The second to fifth columns of Fig. 7a illustrate the dependence of EF coupling with LAI and SM on different temporal averaging lengths. Since the MODIS LAI data are reported at a 4-day interval, we calculate the correlations from EF, LAI, and SMI running means of 8, 16, and 32 days centered on the day when LAI data are available. As expected the correlation increases with averaging length. Nevertheless, the R range stays almost as a constant, suggesting that the heterogeneity in coupling strength does not change with different averaging scales. As to their relative contributions, the vegetation plays a more important role than the SM in the coupling to the EF at most locations at different time scales (Fig. 7b-e). Both R and B values are generally more insensitive when the averaging length exceeds the weekly scale.

Figure 8 shows the results of 16-day averages for dry vs. wet years. Results for other averaging intervals (not shown) are similar to those in Fig. 8. Based on the Palmer Hydrological Drought Index (Heim, 2002) data from NOAA's National Centers for Environmental Information (https://www7.ncdc.noaa.gov/CDO/CDODivisionalSelect.jsp), the warm season of years 2006 and 2011 are relatively dry, while 2007 and 2008 are relatively wet. Stronger coupling strength to the EF can be found at all stations except for E9 during dry years than wet years (Fig. 8a). This result confirms the expectation that coupling strength enhances under drier SM condition in the SM-limited regime. However, the SM contribution (B_{SMI}) displays nonmonotonic changes between dry and wet conditions (Fig. 8b). For instance, B_{SMI} is larger at the CF and E20, but is smaller at E7 and for the domain mean during the wet years. Nonetheless, most sites show greater contribution from LAI than from SM regardless of wetness conditions.

Parallel results of coupling with individual turbulent flux (not shown) are similar to those of coupling with the EF. Overall, the main conclusions regarding the large LA coupling heterogeneities and the greater vegetation impact on the coupling over the same surface type (i.e., pasture/grassland) are still valid when taking into account additional factors, such as turbulent flux fetch, temporal averaging scale, and wetness condition.

6. Conclusions

Heterogeneity in the terrestrial segment of land-atmosphere (LA) coupling in the warm season (May—August) at SGP is studied with multi-year (2004—2011) observations of the near-surface soil moisture (SM) and surface turbulent fluxes from the DOE ARM program and the leaf area index (LAI) from the NASA MODIS instruments. The LA coupling strength is quantified with a new application of multiple linear regression that correlates the surface EF with near-surface SM and LAI. Theoretically, our enhanced LA coupling metric is based on the multidimensional nature of EF-SM relationship, which is consistent with a new framework for differentiating SM-limited and energy-limited evaporation regimes (Haghighi et al., 2018). Our analysis focuses on the daily mean anomalies relative to the climatological monthly averages. This study complements the observational LA coupling database of the traditional SM-EF relationship (Ford et al., 2014; Phillips & Klein, 2014; Phillips et al., 2017) and the recently established LAI-EF relationship (Williams & Torn, 2015; Bagley et al., 2017). Relying on the measurements over the same land type of pasture/grassland, we quantify large spatial variabilities in key coupling variables (e.g., LH, SH, EF, SM, and LAI), in the interaction strength between these variables, and in the relative contributions from the SM and the LAI to the coupling. These large heterogeneities exhibited in various aspects of the LA coupling over the same land type suggest that it may not be appropriate to assume the same LA coupling behaviors over the same land cover at the

SGP. More importantly, these results highlight the challenges in accurately representing surface heterogeneity and LA coupling in regional and global models, as it requires accurate, high resolution, and timely information on soil texture (hydraulic parameters; SM and evapotranspiration (ET)), land cover type, and vegetation health (e.g., LAI) that are difficult to obtain (particularly soils). If any of these are incorrect, it will result in deficiencies in SM-LAI-ET relationships as will be the coupling deduced from the model. Additionally, it is also important to keep in mind the large spatial variabilities in the LA coupling when evaluating global or regional models against domain-mean observations.

This study reveals moderate to weak LA coupling strengths at the analyzed SGP locations. Stronger LA coupling strength is found at all locations by the multi-variable method than by the individual correlations between EF and SM or LAI. Most of their individual regression coefficients of the multi-variable method also are statistically significant, suggesting that both SM and LAI are important factors for the coupling with EF. The relative importance of these two factors, however, varies at different SGP sites due to differences in land use, anthropogenic activities, rooting depth, and soil type. Most sites (6 out of 8) show stronger influence of vegetation than of near-surface SM on the EF. Furthermore, when we examine the impacts on the LH and the SH separately, the LAI dominates the control on the LH oscillations, while the SM and the LAI exert comparable influence on the SH fluctuations. Therefore, the overall greater LAI control on the surface energy partitioning at the SGP is mainly obtained through the LH pathway. This observational evidence implies that better vegetation controls on the EF should be reflected in climate models, and such modifications may contribute to reducing the longstanding LA coupling associated model biases over the SGP (Phillips et al., 2017). An attempt in this direction by Williams et al. (2016) enhances the modeled ET by plants and suppresses the near-surface bare soil evaporation in the off-line Community Land Model 4.5 and the Community Earth System Model 1.2.2 single-column model. Introducing such model changes shows encouraging results (more realistic SM-

EF and LAI-EF relationships as well as smaller surface temperature and precipitation biases) and might also be effective in a global or regional modeling framework.

At the CF, we find moderate coupling strength, and LAI is indeed an important factor besides SM in affecting EF, which is consistent with previous studies (Williams & Torn, 2015; Bagley et al., 2017) in highlighting the vegetation controls in the terrestrial leg of the LA coupling. However, the coupling at the CF cannot represent the range of the SGP sites well due to their great heterogeneity (R: 0.23--0.70). We should note that large uncertainties may exist due to the coarse MODIS LAI data used in the calculation. These findings are insensitive to the wind direction-based flux fetch filter, temporal averaging scale (1 day to 32 days), and dry vs. wet year conditions. Our result emphasizes the pressing need for a better, denser observational network, including point observations of LAI and Normalized Difference Vegetation Index (NDVI), for evaluation of the terrestrial LA coupling in models. Furthermore, the denser network will greatly reduce the risk of sampling biases, which could exist for single-point measurements, due to the naturally large heterogeneities in LA interactions.

It remains largely unclear what mechanisms drive this spatial variability. The differences in the vegetation and soil types, soil depth (surface vs. root zone), and anthropogenic activities can partly explain the variability in coupling. The mesoscale circulation also might be a potentially important factor, as implied by the transition in climate from warmer and drier at the southwest corner of the ARM SGP domain to cooler and moister at the northeast corner. The nonlinear relationship in the LA coupling pathways remains an issue for the multiple linear regression, which may be partly solved by conditional sampling (Ford et al., 2014).

This assessment focused on the terrestrial leg (SM-EF) of LA coupling at the SGP. The metrics established here can be readily applied to measurements at other locations, such as the FLUXNET network (http://www.fluxdata.org), to study LA coupling globally. The statistical approach and metrics demonstrated here are likely to be even more useful for extended LA coupling studies that include the atmosphere and PBL feedback, entrainment, ambient temperature and humidity, and clouds and precipitation, and their relationship with the land surface (SM-EF-LAI) variables of interest. Finally, although the new multiple linear regression application is illustrated here with observational data, it can also be applied readily to model simulations.

Acknowledgments

This work was supported by the Atmospheric Radiation Measurement program (QT, SX, YZ, LR, and KG) and the Regional and Global Climate Modeling and Atmospheric System Research programs (YZ, and TJP) of the U.S. Department of Energy (DOE) under the auspices of the U.S. DOE by Lawrence Livermore National Laboratory under contract DE-AC52-07NA27344. The authors thank Paul Dirmeyer, Ian Williams, and Karl Taylor for their helpful comments and suggestions. The ARM data were obtained at www.arm.gov from the sgparmbestnsX1.c1 and sgparmbe2dgridX1.c1 data stream. The MCD15A3H level 4 leaf area index data were retrieved from the NASA EOSDIS Land Processes Distributed Active Archive Center (LP DAAC), USGS/Earth Resources Observation and Science (EROS) Center, Sioux Falls, South Dakota, (https://lpdaac.usgs.gov). LLNL-JRNL-745706.

References

Bagley, J. E., Kueppers, L. M., Billesbach, D. P., Williams, I. N., Biraud, S. C., & Torn, M. S. (2017). The influence of land cover on surface energy partitioning and evaporative fraction regimes in the U.S. Southern Great Plains. *Journal of Geophysical Research: Atmospheres*, 2017JD026740. https://doi.org/10.1002/2017JD026740

Barnes, S. L. (1964). A Technique for Maximizing Details in Numerical Weather Map Analysis. *Journal of Applied Meteorology*, *3*(4), 396–409. https://doi.org/10.1175/1520-0450(1964)003<0396:ATFMDI>2.0.CO;2

Betts, A. K. (2004). Understanding Hydrometeorology Using Global Models. *Bulletin of the American Meteorological Society*, *85*(11), 1673–1688. https://doi.org/10.1175/BAMS-85-11-1673

Betts, A. K. (2009). Land-Surface-Atmosphere Coupling in Observations and Models. *Journal of*

Advances in Modeling Earth Systems, *1*(3), 4. https://doi.org/10.3894/JAMES.2009.1.4

Betts, A. K., Desjardins, R., Beljaars, A. C. M., & Tawfik, A. (2015). Observational study of land-surface-cloud-atmosphere coupling on daily timescales. *Frontiers in Earth Science*, *3*, 13. https://doi.org/10.3389/feart.2015.00013

Budyko, M. I. (1974). *Climate and Life*. New York, NY: Academic Press.

Cook, D. R. (2018). *Energy Balance Bowen Ratio (EBBR) Handbook* (DOE/SC-ARM/TR-037 No. DOE/SC-ARM/TR-037) (p. 30). ARM Climate Research Facility. Retrieved from https://www.arm.gov/publications/tech_reports/handbooks/ebbr_handbook.pdf

Dirmeyer, P. A. (2011). The terrestrial segment of soil moisture–climate coupling. *Geophysical Research Letters*, *38*(16), L16702. https://doi.org/10.1029/2011GL048268

Dirmeyer, P. A., Cash, B. A., Kinter, J. L., Stan, C., Jung, T., Marx, L., et al. (2012). Evidence for Enhanced Land–Atmosphere Feedback in a Warming Climate. *Journal of Hydrometeorology*, *13*(3), 981–995. https://doi.org/10.1175/JHM-D-11-0104.1

Dirmeyer, P. A., Jin, Y., Singh, B., & Yan, X. (2013). Trends in Land–Atmosphere Interactions from CMIP5 Simulations. *Journal of Hydrometeorology*, *14*(3), 829–849. https://doi.org/10.1175/JHM-D-12-0107.1

Ek, M. B., & Holtslag, A. a. M. (2004). Influence of Soil Moisture on Boundary Layer Cloud Development. *Journal of Hydrometeorology*, *5*(1), 86–99. https://doi.org/10.1175/1525-7541(2004)005<0086:IOSMOB>2.0.CO;2

Ferguson, C. R., Wood, E. F., & Vinukollu, R. K. (2012). A Global Intercomparison of Modeled and Observed Land–Atmosphere Coupling. *Journal of Hydrometeorology*, *13*(3), 749–784. https://doi.org/10.1175/JHM-D-11-0119.1

Findell, K. L., & Eltahir, E. A. B. (2003). Atmospheric Controls on Soil Moisture–Boundary Layer Interactions. Part II: Feedbacks within the Continental United States. *Journal of Hydrometeorology*, *4*(3), 570–583. https://doi.org/10.1175/1525-7541(2003)004<0570:ACOSML>2.0.CO;2

Findell, K. L., Gentine, P., Lintner, B. R., & Kerr, C. (2011). Probability of afternoon precipitation in eastern United States and Mexico enhanced by high evaporation. *Nature Geoscience*, *4*(7), 434–439. https://doi.org/10.1038/ngeo1174

Fisher, R. A. (1921). On the “Probable Error” of a Coefficient of Correlation Deduced from a Small Sample. Retrieved from https://digital.library.adelaide.edu.au/dspace/handle/2440/15169

Ford, T. W., Wulff, C. O., & Quiring, S. M. (2014). Assessment of observed and model-derived soil moisture-evaporative fraction relationships over the United States Southern Great Plains. *Journal of Geophysical Research: Atmospheres*, *119*(11), 2014JD021490. https://doi.org/10.1002/2014JD021490

Gentine, P., Holtslag, A. A. M., D’Andrea, F., & Ek, M. (2013). Surface and Atmospheric Controls on the Onset of Moist Convection over Land. *Journal of Hydrometeorology*, *14*(5), 1443–1462.

https://doi.org/10.1175/JHM-D-12-0137.1

Govindjee. (2012). *Photosynthesis V2: Development, Carbon Metabolism, and Plant Productivity*. Elsevier.

Guo, Z., Dirmeyer, P. A., Koster, R. D., Sud, Y. C., Bonan, G., Oleson, K. W., et al. (2006). GLACE: The Global Land–Atmosphere Coupling Experiment. Part II: Analysis. *Journal of Hydrometeorology*, *7*(4), 611–625. https://doi.org/10.1175/JHM511.1

Haghighi, E., Short Gianotti, D. J., Akbar, R., Salvucci, G. D., & Entekhabi, D. (2018). Soil and Atmospheric Controls on the Land Surface Energy Balance: A Generalized Framework for Distinguishing Moisture- and Energy-Limited Evaporation Regimes. *Water Resources Research*, *54*, 1831–1851. https://doi.org/10.1002/2017WR021729

Heim, R. R. (2002). A Review of Twentieth-Century Drought Indices Used in the United States. *Bulletin of the American Meteorological Society*, *83*(8), 1149–1166. https://doi.org/10.1175/1520-0477-83.8.1149

Klein, S. A., Jiang, X., Boyle, J., Malyshev, S., & Xie, S. (2006). Diagnosis of the summertime warm and dry bias over the U.S. Southern Great Plains in the GFDL climate model using a weather forecasting approach. *Geophysical Research Letters*, *33*(18), L18805. https://doi.org/10.1029/2006GL027567

Koster, R. D., Dirmeyer, P. A., Hahmann, A. N., Ijpelaar, R., Tyahla, L., Cox, P., & Suarez, M. J. (2002). Comparing the Degree of Land–Atmosphere Interaction in Four Atmospheric General Circulation Models. *Journal of Hydrometeorology*, *3*(3), 363–375. https://doi.org/10.1175/1525-7541(2002)003<0363:CTDOLA>2.0.CO;2

Koster, R. D., Dirmeyer, P. A., Guo, Z., Bonan, G., Chan, E., Cox, P., et al. (2004). Regions of Strong Coupling Between Soil Moisture and Precipitation. *Science*, *305*(5687), 1138–1140. https://doi.org/10.1126/science.1100217

Koster, R. D., Sud, Y. C., Guo, Z., Dirmeyer, P. A., Bonan, G., Oleson, K. W., et al. (2006). GLACE: The Global Land–Atmosphere Coupling Experiment. Part I: Overview. *Journal of Hydrometeorology*, *7*(4), 590–610. https://doi.org/10.1175/JHM510.1

Kutner, M. H., Neter, J., Nachtsheim, C. J., & Li, W. (2004). *Applied Linear Statistical Models* (5th International edition). Boston, Mass.: McGraw-Hill Education.

Ma, H. -Y., Klein, S. A., Xie, S., Zhang, C., Tang, S., Tang, Q., et al. (2018). CAUSES: On the Role of Surface Energy Budget Errors to the Warm Surface Air Temperature Error Over the Central United States. *Journal of Geophysical Research: Atmospheres*, *123*(5), 2888–2909. https://doi.org/10.1002/2017JD027194

Moene, A. F., & van Dam, J. C. (2014). *Transport in the Atmosphere-Vegetation-Soil Continuum*. Cambridge University Press.

Myneni, R. (2015). Leaf Area Index and Fractional Photosynthetically Active Radiation, *MCD15A3H V006*, NASA EOSDIS Land Processes DAAC, USGS Earth Resources Observation and

Science (EROS) Center, Sioux Falls, South Dakota (https://lpdaac.usgs.gov). https://doi.org/10.5067/MODIS/MCD15A3H.006

Oleson, K., Lawrence, M., Bonan, B., Drewniak, B., Huang, M., Koven, D., et al. (2013). Technical description of version 4.5 of the Community Land Model (CLM). https://doi.org/10.5065/D6RR1W7M

Phillips, T. J., & Klein, S. A. (2014). Land-atmosphere coupling manifested in warm-season observations on the U.S. southern great plains. *Journal of Geophysical Research: Atmospheres*, *119*(2), 2013JD020492. https://doi.org/10.1002/2013JD020492

Phillips, T. J., Klein, S. A., Ma, H.-Y., Tang, Q., Xie, S., Williams, I. N., et al. (2017). Using ARM Observations to Evaluate Climate Model Simulations of Land-Atmosphere Coupling on the U.S. Southern Great Plains. *Journal of Geophysical Research: Atmospheres*, *122*(21), 2017JD027141. https://doi.org/10.1002/2017JD027141

Qian, Y., Huang, M., Yang, B., & Berg, L. K. (2013). A Modeling Study of Irrigation Effects on Surface Fluxes and Land–Air–Cloud Interactions in the Southern Great Plains. *Journal of Hydrometeorology*, *14*(3), 700–721. https://doi.org/10.1175/JHM-D-12-0134.1

Santanello, J. A., Friedl, M. A., & Ek, M. B. (2007). Convective Planetary Boundary Layer Interactions with the Land Surface at Diurnal Time Scales: Diagnostics and Feedbacks. *Journal of Hydrometeorology*, *8*(5), 1082–1097. https://doi.org/10.1175/JHM614.1

Santanello, J. A., Peters-Lidard, C. D., & Kumar, S. V. (2011). Diagnosing the Sensitivity of Local Land–Atmosphere Coupling via the Soil Moisture–Boundary Layer Interaction. *Journal of Hydrometeorology*, *12*(5), 766–786. https://doi.org/10.1175/JHM-D-10-05014.1

Seneviratne, S. I., Lüthi, D., Litschi, M., & Schär, C. (2006). Land–atmosphere coupling and climate change in Europe. *Nature*, *443*(7108), 205–209. https://doi.org/10.1038/nature05095

Seneviratne, S. I., Corti, T., Davin, E. L., Hirschi, M., Jaeger, E. B., Lehner, I., et al. (2010). Investigating soil moisture–climate interactions in a changing climate: A review. *Earth-Science Reviews*, *99*(3–4), 125–161. https://doi.org/10.1016/j.earscirev.2010.02.004

Tang, Q., & Xie, S. (2015a). *2D Gridded Surface Data Value-Added Product* (DOE/SC-ARM/TR-152 No. DOE/SC-ARM/TR-152) (p. 23). ARM Climate Research Facility. Retrieved from http://www.arm.gov/publications/tech_reports/doe-sc-arm-tr-152.pdf

Tang, Q., & Xie, S. (2015b). *Station-based Surface Data Value-Added Product* (DOE/SC-ARM/TR-151 No. DOE/SC-ARM/TR-151) (p. 23). ARM Climate Research Facility. Retrieved from http://www.arm.gov/publications/tech_reports/doe-sc-arm-tr-151.pdf?id=966

Taylor, C. M., de Jeu, R. A. M., Guichard, F., Harris, P. P., & Dorigo, W. A. (2012). Afternoon rain more likely over drier soils. *Nature*, *489*(7416), 423–426. https://doi.org/10.1038/nature11377

Taylor, K. E. (2001). Summarizing multiple aspects of model performance in a single diagram. *Journal of Geophysical Research: Atmospheres*, *106*(D7), 7183–7192. https://doi.org/10.1029/2000JD900719

Taylor, K. E., Stouffer, R. J., & Meehl, G. A. (2012). An Overview of CMIP5 and the Experiment Design. *Bulletin of the American Meteorological Society*, *93*(4), 485–498. https://doi.org/10.1175/BAMS-D-11-00094.1

Van Weverberg, K., Morcrette, C. J., Petch, J., Klein, S. A., Ma, H. -Y., Zhang, C., et al. (2018). CAUSES: Attribution of Surface Radiation Biases in NWP and Climate Models near the U.S. Southern Great Plains. *Journal of Geophysical Research: Atmospheres*, *123*(7), 3612–3644. https://doi.org/10.1002/2017JD027188

Wei, J., & Dirmeyer, P. A. (2010). Toward understanding the large-scale land-atmosphere coupling in the models: Roles of different processes. *Geophysical Research Letters*, *37*(19), L19707. https://doi.org/10.1029/2010GL044769

Williams, I. N., & Torn, M. S. (2015). Vegetation controls on surface heat flux partitioning, and land-atmosphere coupling. *Geophysical Research Letters*, 2015GL066305. https://doi.org/10.1002/2015GL066305

Williams, I. N., Lu, Y., Kueppers, L. M., Riley, W. J., Biraud, S. C., Bagley, J. E., & Torn, M. S. (2016). Land-atmosphere coupling and climate prediction over the U.S. Southern Great Plains. *Journal of Geophysical Research: Atmospheres*, *121*(20), 2016JD025223. https://doi.org/10.1002/2016JD025223

Xie, S., McCoy, R. B., Klein, S. A., Cederwall, R. T., Wiscombe, W. J., Jensen, M. P., et al. (2010). CLOUDS AND MORE: ARM Climate Modeling Best Estimate Data. *Bulletin of the American Meteorological Society*, *91*(1), 13–20. https://doi.org/10.1175/2009BAMS2891.1

Zhang, Y., & Klein, S. A. (2013). Factors Controlling the Vertical Extent of Fair-Weather Shallow Cumulus Clouds over Land: Investigation of Diurnal-Cycle Observations Collected at the ARM Southern Great Plains Site. *Journal of the Atmospheric Sciences*, *70*(4), 1297–1315. https://doi.org/10.1175/JAS-D-12-0131.1

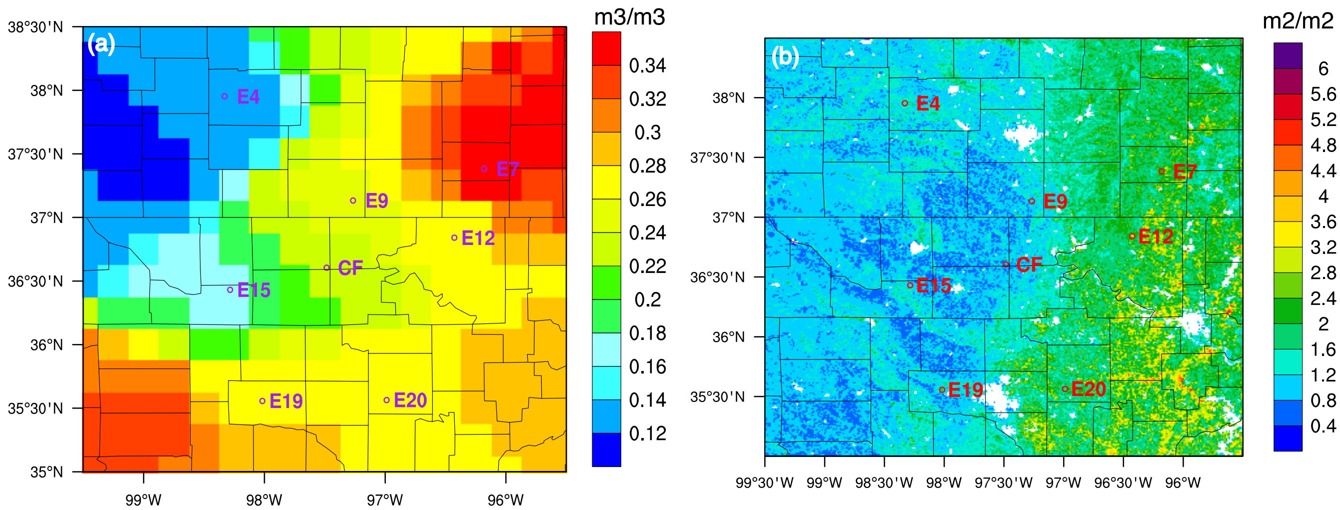

Figure 1. Mean warm-season (May—August) geographic patterns of years 2004—2011 for **(a)** EBBR soil moisture (unit: volumetric m^3/m^3) at 0.25° x 0.25° resolution and **(b)** MODIS LAI (unit: m^2/m^2) at 500m x 500m resolution. Site locations used in the study are marked by circles. See Table 1 for site names.

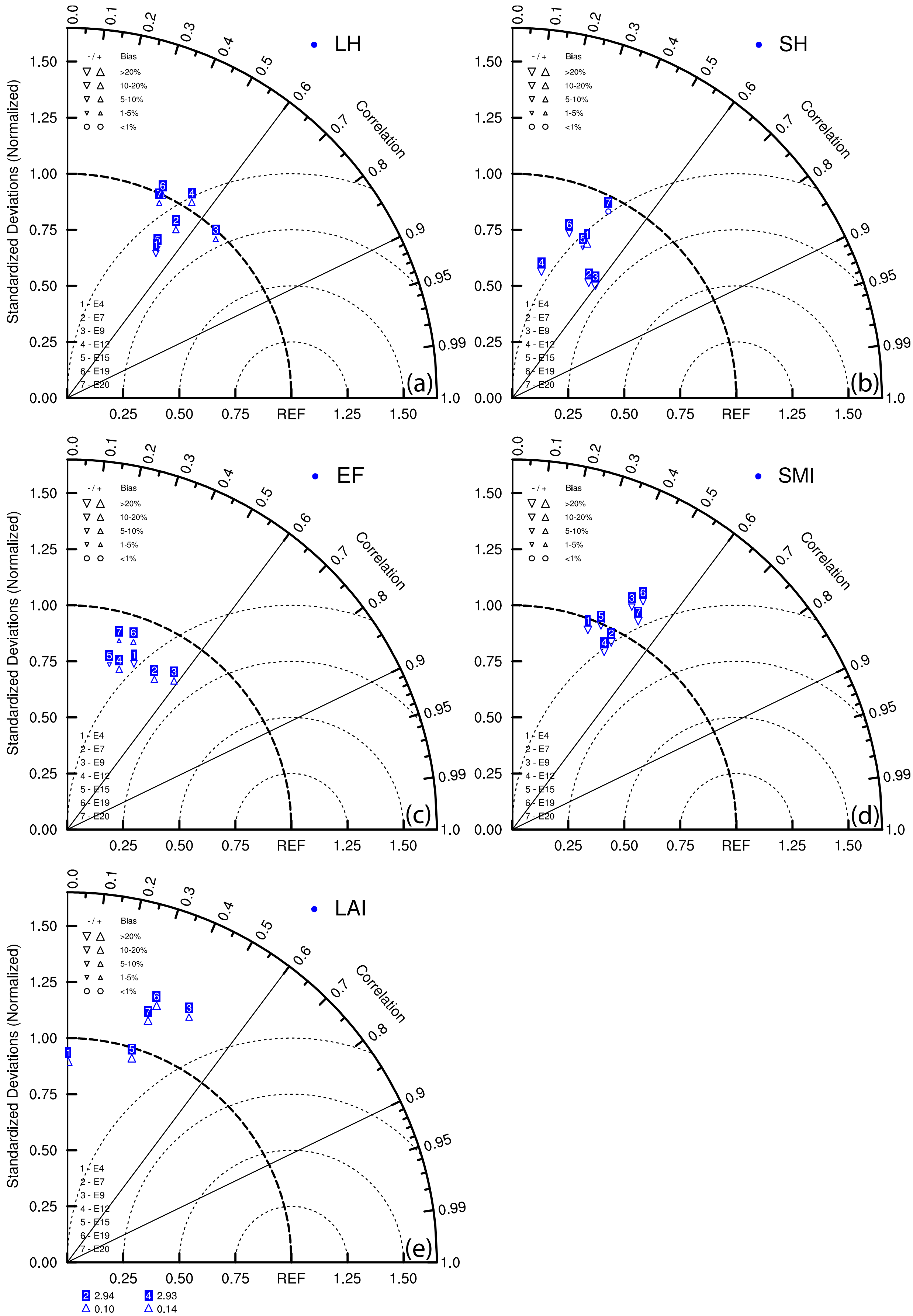
LH
SH
EF
SMI
LAI
Standardized Deviations (Normalized)
Correlation
REF
- / +
Bias
>20%
10-20%
5-10%
1-5%
<1%
1 - E4
2 - E7
3 - E9
4 - E12
5 - E15
6 - E19
7 - E20
(a)
(b)
(c)
(d)
(e)
2 2.94
0.10
4 2.93
0.14

Figure 2. Taylor diagrams for key LA coupling variables: **(a)** latent heat (LH) flux, **(b)** sensible heat (SH) flux, **(c)** evaporative fraction (EF), **(d)** soil moisture index (SMI), and **(e)** leaf area index (LAI) at different SGP sites compared to the CF, which is denoted by the reference point (1, 0). Standard deviations are normalized by that of the CF. Biases are indicated by the size and shape of the markers (top left of each panel). All the correlations pass the two-tailed t-test at a 95% confidence level except for the LAI at sites E4 and E7. The normalized standard deviations of LAI at E7 and E12 are off the charts, and hence their numbers are labeled on the bottom of panel **(e)**.

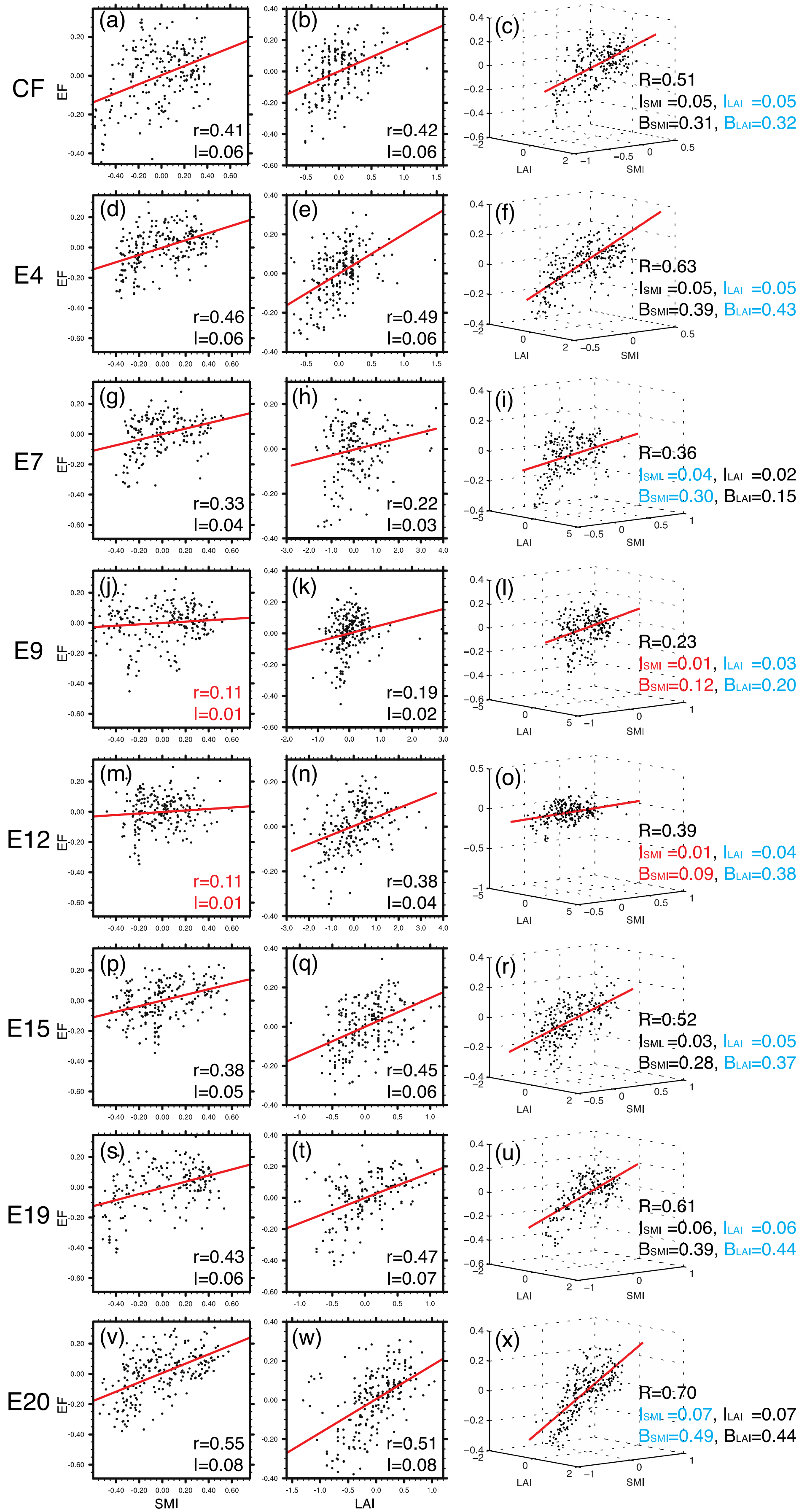
CF
E4
E7
E9
E12
E15
E19
E20
EF
SMI
LAI
(a) r=0.41 I=0.06
(b) r=0.42 I=0.06
(c) R=0.51 ISMI =0.05, ILAI =0.05 BSMI=0.31, BLAI=0.32
(d) r=0.46 I=0.06
(e) r=0.49 I=0.06
(f) R=0.63 ISMI =0.05, ILAI =0.05 BSMI=0.39, BLAI=0.43
(g) r=0.33 I=0.04
(h) r=0.22 I=0.03
(i) R=0.36 ISMI =0.04, ILAI =0.02 BSMI=0.30, BLAI=0.15
(j) r=0.11 I=0.01
(k) r=0.19 I=0.02
(l) R=0.23 ISMI =0.01, ILAI =0.03 BSMI=0.12, BLAI=0.20
(m) r=0.11 I=0.01
(n) r=0.38 I=0.04
(o) R=0.39 ISMI =0.01, ILAI =0.04 BSMI=0.09, BLAI=0.38
(p) r=0.38 I=0.05
(q) r=0.45 I=0.06
(r) R=0.52 ISMI =0.03, ILAI =0.05 BSMI=0.28, BLAI=0.37
(s) r=0.43 I=0.06
(t) r=0.47 I=0.07
(u) R=0.61 ISMI =0.06, ILAI =0.06 BSMI=0.39, BLAI=0.44
(v) r=0.55 I=0.08
(w) r=0.51 I=0.08
(x) R=0.70 ISMI =0.07, ILAI =0.07 BSMI=0.49, BLAI=0.44

Figure 3. Scatter plots of daily averages (May—August of years 2004—2011) of evaporative fraction (EF) vs. soil moisture index (SMI) (first column), leaf area index (LAI) (second column), and SMI and LAI (third column) at the 8 ARM SGP sites (rows). The climatological monthly means are subtracted from the raw time series. Red lines represent the least squares regression lines. Simple (r) and multiple (R) correlation coefficients, sensitivity indices (I), and standardized regression coefficients (B) are denoted on each panel. For the multiple regression metric, the larger I or B numbers are highlighted in blue (note that SMI and LAI values may appear the same due to round off errors). Statistically insignificant quantities at a 95% confidence level are in red.

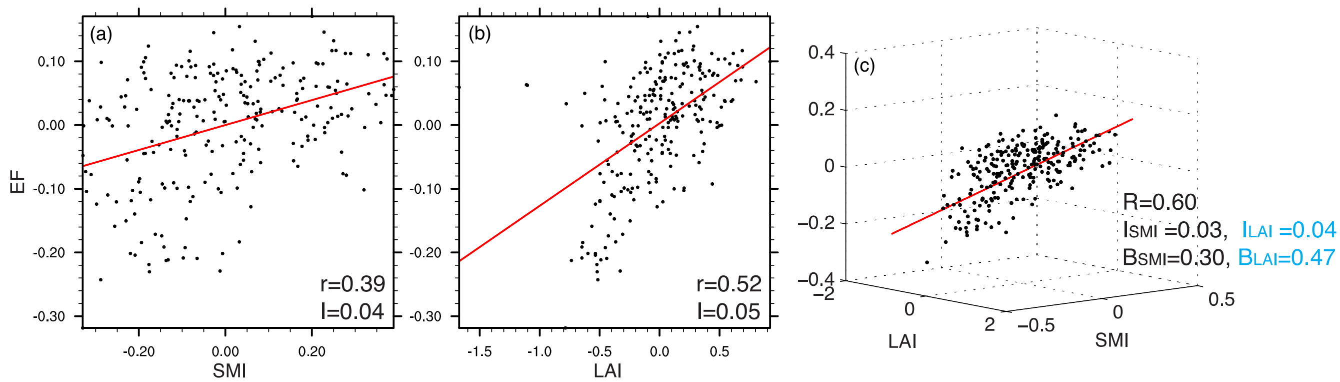

Figure 4. Same as Fig. 3, but for domain means averaged over the 8 ARM SGP sites.

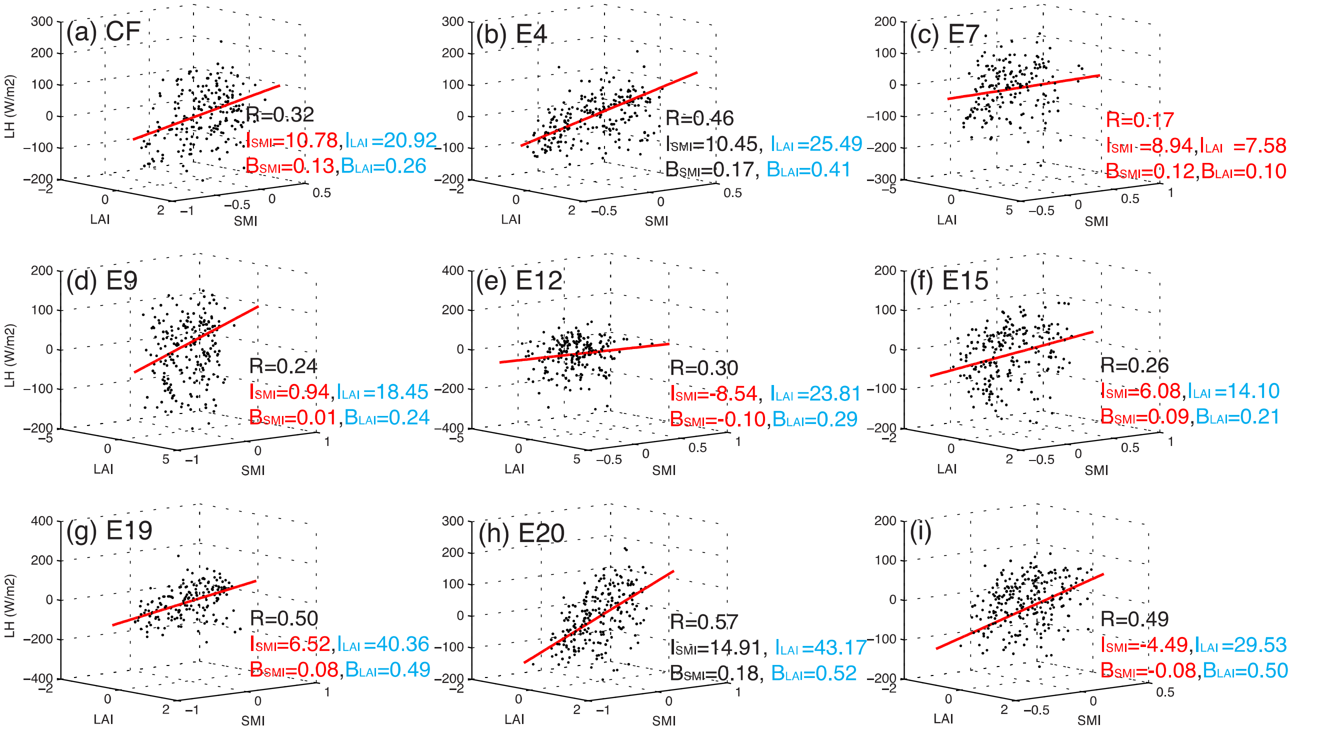

Figure 5. Same as Fig. 3, but for scatter plots of latent heat (LH) vs. SMI and LAI for the 8 stations as well as the domain averages. The domain-mean results are shown on panel **(i)**.

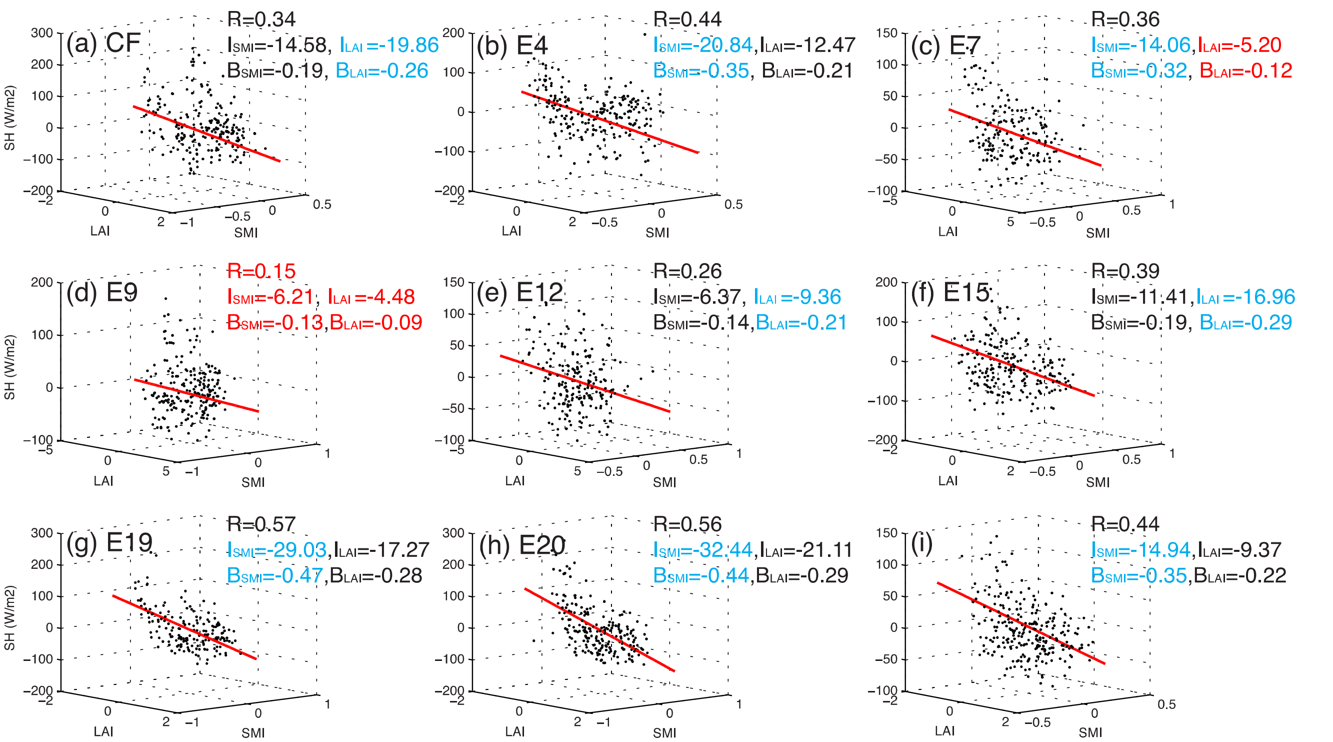

Figure 6. Same as Fig. 5, but for scatter plots of sensible heat (SH) flux vs. SMI and LAI. Note that the I and B numbers with larger absolute values are in blue.

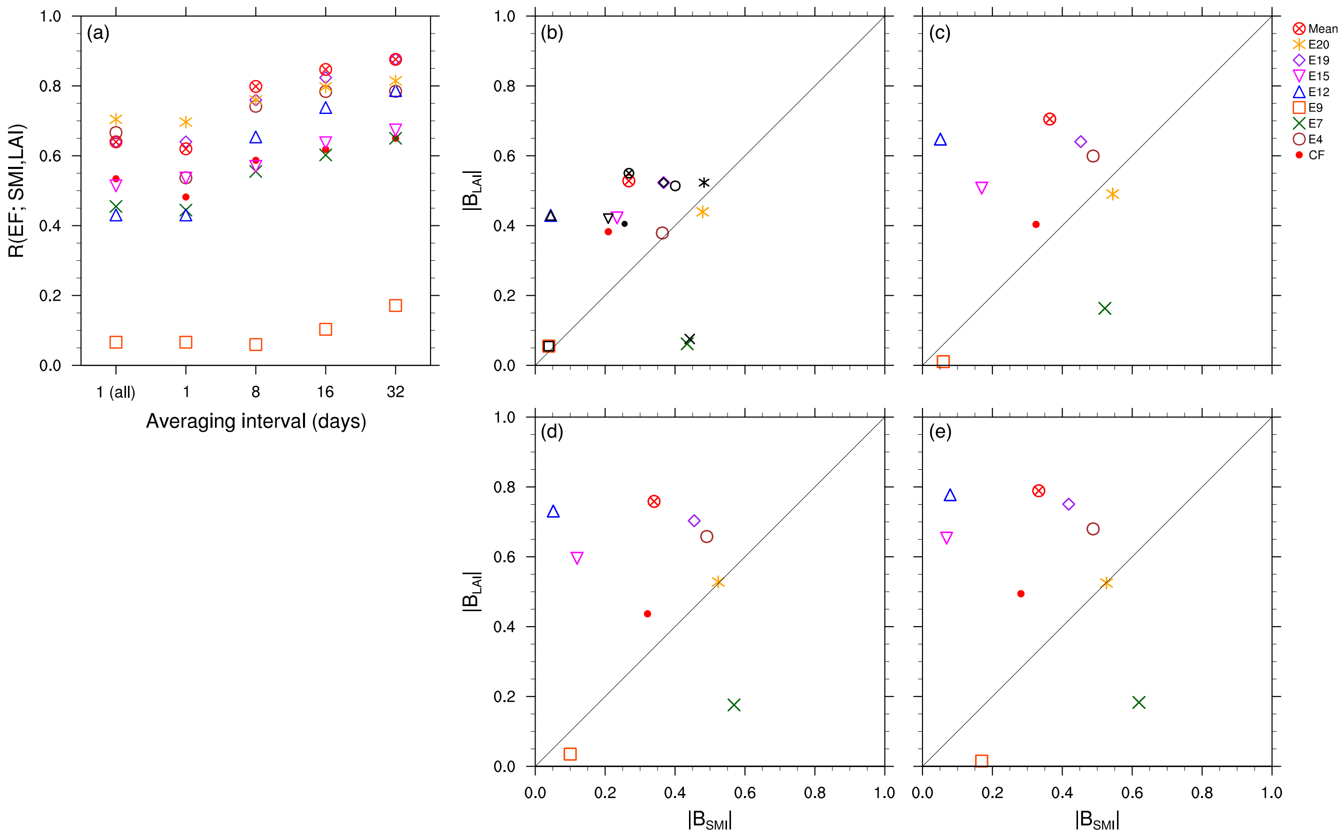

Figure 7. (a) Multiple correlation coefficient R(EF; SMI, LAI) for (May—August of years 2004—2011) as a function of averaging intervals. All columns show results with wind direction filter except for the first column. Scatter plots of absolute values of standardized regression coefficients B_{LAI} vs. B_{SMI} with a **(b)** 1-day, **(c)** 8-day, **(d)** 16-day, and **(e)** 32-day averaging length. Color symbols represent results with the wind direction filter, while black symbols indicate those without the wind direction filter. The black lines denote the 1:1 line.

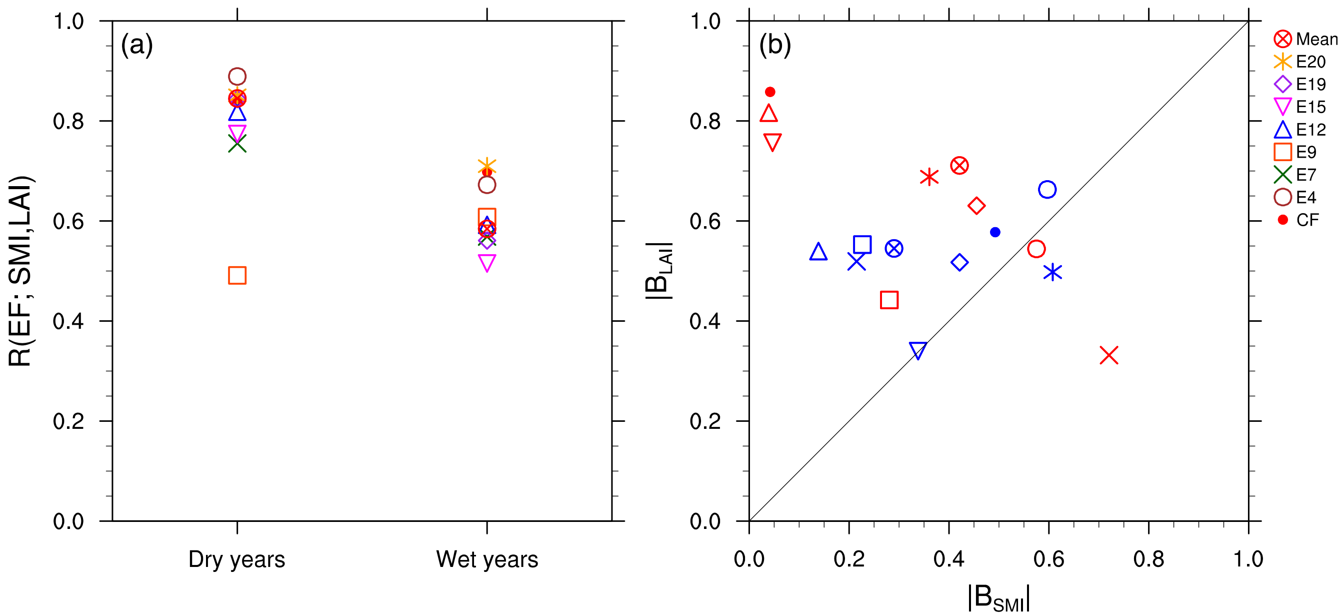

Figure 8. Same as Fig. 7ab, but for comparisons of 16-day averaging results between dry (2006 and 2011) and wet (2007 and 2008) years. In panel **(b)**, results from dry years are in red, whereas those from wet years in blue.

Table 1. Summary of correlation coefficients between SMI and LAI denoted by r(SMI, LAI), number of data points denoted by N, surface vegetation, soil types, and wind directions for better EBBR flux measurements at different locations. Data point numbers in Figs. 3--6 are the same as shown here because we apply the same screening algorithm for all methods. Statistically insignificant numbers at a 95% confidence level are in red.

Sites		N	r(SMI, LAI)	Surf. Type	Soil Type	Wind direction (degree) (Cook, 2018)
Abbr.	Location					
CF/E13	Lamont, OK	208	0.30	Pasture (ungrazed)	Silty Loam	0—52, 142—194, 328—360
E4	Plevna, KS	228	0.15	Rangeland (ungrazed)	Fine Sandy Loam	0—158, 202—360
E7	Elk Falls, KS	179	0.21	Pasture	Silty Loam	0—244, 296—360
E9	Ashton, KS	215	0.07	Pasture	Loam	0—360
E12	Pawhuska, OK	208	0.03	Native Tallgrass Prairie	Sandy Loam	0—360
E15	Ringwood, OK	216	0.28	Pasture	Sandy Loam	133—360
E19	El Reno, OK	174	0.08	Pasture (ungrazed)	Silty Loam	0—133, 151—360
E20	Meeker, OK	221	0.15	Pasture	Silty Loam	0—230, 310—360
Mean		246	0.18			